RSC Advances

ROYAL SOCIETY
OF CHEMISTRY

www.rsc.org/advances

Journal Name

Dynamic Article Links ▶

ARTICLE TYPE

Flexible Janus Nanofiber: a Feasible Route to Realize Simultaneously Tuned Magnetism and Enhanced Color-Tunable Luminescence Bifunctionality

Xuejiao Zhou, Qianli Ma, Xiangting Dong*, Jinxian Wang, Wensheng Yu, and Guixia Liu

Novel magnetic-fluorescent bifunctional Janus nanofibers with high luminescent intensity and tunable luminescent color have been successfully fabricated by electrospinning technology using a specially designed parallel spinneret. The Janus nanofiber is composed of Fe_3O_4/polyvinyl pyrrolidone (PVP) as
10 one strand nanofiber and $[Dy(BA)_3phen+Eu(BA)_3phen]$/PVP as the other strand nanofiber. The morphology and properties of the final products have been investigated in detail by X-ray diffractometry (XRD), scanning electron microscopy (SEM), energy dispersive spectrometry (EDS), transmission electron microscopy (TEM), vibrating sample magnetometry (VSM) and photoluminescence (PL) spectroscopy. The results reveal that the Janus nanofibers possess superior magnetic and luminescent
15 properties due to their special nanostructure. Tunable colors from greenish blue to white to yellowish pink can be realized in the flexible Janus nanofibers by varying the mass ratio of $Dy(BA)_3phen$ to $Eu(BA)_3phen$, and furthermore, it is the first time that white-light-emitting flexible Janus nanofibers are achieved using rare earth complexes as luminescent centers. The impact of different amounts of Fe_3O_4 nanoparticles on the luminescent color and intensity of the Janus nanofibers is in-depth investigated. The
20 new type of magnetic and color-tunable bifunctional Janus nanofibers have potential applications in the fields of bio-medicine, nanotechnology, and color displays, etc. due to their excellent magnetic-fluorescent properties, tunable color and flexibility.

Introduction

Nowadays, color-tunable luminescent materials have attracted
25 considerable attention owing to their wide range of applications, such as light-emitting diodes (LEDs), transducers, resonators, flat panel displays and full-color displays.[1-5] Generally, color-tunable luminescent materials and white light-emitting materials are prepared by using Dy^{3+} and Eu^{3+} ions (rare earth ions) doped
30 inorganic compounds as the luminescent centers due to the abundant emission colors based on their 4f electrons transitions, such as $NaGaF_4$: Dy^{3+}, Eu^{3+} nanophosphors, $SrAl_2O_4$: Dy^{3+}, Eu^{3+} phosphors, and $GdNbO_4$: Dy^{3+}, Eu^{3+} phosphors, etc.[6-9] As far as we know, there are no reports concerning the preparation of
35 $Dy(BA)_3phen$ and $Eu(BA)_3phen$ complexes doped one-dimensional (1D) composite nanofibers. Therefore, it is a worthwhile subject of study to explore new-typed of 1D color-tunable luminescent and white light-emitting nanomaterials.

Magnetic-luminescent bifunctional composite nanomaterials
40 have been applied in medical diagnostics, optical imaging, nanodevice, etc.[10-14] In recent years, some preparations of Fe_3O_4@rare earth (RE) complex core-shell structure nanoparticles (NPs) have been reported.[15-19] At present, some 1D magnetic-luminescent bifunctional nanomaterials have been
45 prepared, including Fe_2O_3/$Eu(DBM)_3(Bath)$/PVP composite nanofibers, Fe_3O_4/$Eu(BA)_3phen$/PMMA composite nanoribbons,

etc.[20, 21] In their papers, however, magnetic-luminescent bifunctional composite nanomaterials usually have poor fluorescence properties because Fe_3O_4 or Fe_2O_3 NPs directly
50 contacts with the RE luminescent compounds, which restrict the use of these magnetic-luminescent bifunctional nanomaterials to promising extensive photophysical applications and practical uses. Therefore, luminescent and magnetic materials should be effectively isolated to avoid direct contact if the strong
55 luminescence of the magnetic and color-tunable bifunctional composite nanofibers is achieved. We were inspired by the reports on the Janus particles.[22] Janus particles have two distinguished surfaces/chemistries on the two sides. Upon the unique feature of the asymmetry dual-sided Janus structure, we
60 have successfully designed and fabricated the Janus nanofibers in our previous work.[23-25]

Electrospinning represents an outstanding technique to process viscous solutions or melts into continuous fibers or ribbons with 1D nanostructure.[26-28] The electrospun products have been
65 applied in many areas such as filtration, optical and chemical sensors, biological scaffolds, electrode materials, drug delivery materials, photocatalysts and nanocables.[29-35] Accordingly, here we employed electrospinning method to prepare magnetic and color-tunable bifunctional
70 $[Fe_3O_4$/PVP$]//[(Dy(BA)_3phen+Eu(BA)_3phen)$/PVP$]$ Janus

nanofibers with new 1D structure in this paper. For the Janus nanofibers, its one strand nanofiber is composed of template PVP containing Fe_3O_4 NPs (namely Fe_3O_4/PVP nanofiber), and the other strand nanofiber consists of PVP containing $Dy(BA)_3$phen

5 and Eu(BA)_3phen complexes (namely [Dy(BA)_3phen+Eu(BA)_3phen]/PVP nanofiber). This new-type 1D nanostructure can successfully realize the effective separation of Fe_3O_4 NPs from the RE complexes (include $Dy(BA)_3$phen and $Eu(BA)_3$phen complexes), and this great morphology of

10 bifunctional nanofibers will be obtained with excellent magnetism and color-tunable luminescence. To the best of our knowledge, the novel magnetic and color-tunable bifunctional Janus nanofibers have not been found in any literature. Full characterization and detailed studies of the magnetic and color-

15 tunable properties of these Janus nanofibers were discussed.

Experimental Sections

Materials

Polyvinyl pyrrolidone (PVP, Mw ≈ 90,000), benzoic acid (BA), 1,10-phenanthroline (phen), $FeCl_3 \cdot 6H_2O$, $FeSO_4 \cdot 7H_2O$, NH_4NO_3,

20 polyethyleneglycol (PEG, Mw ≈ 20,000), ammonia, anhydrous ethanol, oleic acid (OA) and N,N-dimethylformamide (DMF) were of analytical grade. The purity of Eu_2O_3 and Dy_2O_3 was 99.99 %. All chemicals were directly used as received without further purification.

25 ### Preparation of Fe_3O_4 NPs by coprecipitation method

Fe_3O_4 NPs were obtained via a facile coprecipitation synthetic method,[36] and PEG was used as the protective agent to prevent the particles from aggregation. One typical synthetic procedure was as follows: 8.0800 g of $Fe(NO)_3 \cdot 9H_2O$, 2.7800 g of

30 $FeSO_4 \cdot 7H_2O$, 4.0400 g of NH_4NO_3, and 1.9000 g of PEG were added into 100 mL of deionized water to form uniform solution under vigorous stirring at 50 °C. To prevent the oxidation of Fe^{2+} ions, the reactive mixture was kept under argon atmosphere. After the mixture had been bubbled with argon for 30 min, 0.1 mol/L of

35 $NH_3 \cdot H_2O$ was added dropwise into the mixture to adjust the pH value above 11. Then the system was continuously bubbled with argon for 20 min at 50 °C, and black precipitates were formed. The precipitates were collected from the solution by magnetic separation, washed with the mixed solution of deionized water

40 and anhydrous ethanol for three times, and then dried in an electric vacuum oven at 60 °C for 12 h.

To improve the monodispersity, stability and solubility of Fe_3O_4 NPs in the spinning solution, the as-prepared Fe_3O_4 NPs were coated with OA as below: 2.0000 g of the as-prepared Fe_3O_4

45 NPs were ultrasonically dispersed in 100 mL of deionized water for 20 min. The suspension was heated to 80 °C under argon atmosphere with vigorous mechanical stirring for 30 min, and then 1.5 mL of OA was slowly added into the above suspension. Reaction was stopped after heating and stirring the mixture for 40

50 min. The precipitates were removed from the solution by magnetic separation, and then dried in an electric vacuum oven at 60 °C for 6 h.

Synthesis of $Dy(BA)_3$phen and $Eu(BA)_3$phen complexes

$Dy(BA)_3$phen powders were synthesized according to the

55 traditional method as described in the reference.[37] 1.8650 g of

Dy_2O_3 was dissolved in 10 mL of concentrated nitric acid and then crystallized via evaporation of excess nitricacid and water by heating, and $Dy(NO_3)_3 \cdot 6H_2O$ powders were acquired. $Dy(NO_3)_3$ ethanol solution was prepared by adding 20 mL of anhydrous

60 ethanol into the above $Dy(NO_3)_3 \cdot 6H_2O$. 3.6600 g of BA and 1.8000 g of phen were dissolved in 200 mL of ethanol. The $Dy(NO_3)_3$ ethanol solution was then added into the mixed solution of BA and phen with magnetic agitation for 3 h at 60 °C. The precipitates were collected by filtration and dried at 60 °C for

65 12 h. The synthetic method of $Eu(BA)_3$phen complex was similar to the above method, except that the used dosages of Eu_2O_3, BA and phen were 1.7600 g, 3.6640 g and 1.8020 g, respectively.

Preparations of spinning solutions for fabricating [Fe_3O_4/PVP]//[(Dy(BA)_3phen+Eu(BA)_3phen)/PVP] Janus

70 nanofibers and Fe_3O_4/[Dy(BA)_3phen+Eu(BA)_3phen]/PVP composite nanofibers

Two different kinds of spinning solutions were prepared to fabricate Janus nanofibers. The spinning solution for one strand nanofiber of Janus nanofibers consisted of $Dy(BA)_3$phen,

75 $Eu(BA)_3$phen, PVP, and DMF (denoted as spinning solutions A). A series of [Dy(BA)_3phen+Eu(BA)_3phen]/PVP spinning solutions with different mass percentages of $Eu(BA)_3$phen were prepared. Herein, the mass percentage of $Dy(BA)_3$phen to PVP was settled as 10 % in all the spinning solutions A, which was because the

80 luminescent intensity of $Dy(BA)_3$phen in PVP matrix was the strongest, as indicated in Fig. S1, Supplementary. In order to fabricate color-tunable Janus nanofibers, the mass percentages of $Eu(BA)_3$phen to PVP were settled as 0 %, 0.5 %, 1 %, 2 %, and 3 %, respectively. $Dy(BA)_3$phen and $Eu(BA)_3$phen complexes

85 were added into 4.0000 g of DMF, and then 1.0000g of PVP powder was dissolved into the above solutions under magnetic stirring for 12 h.

The other spinning solution for one strand nanofiber of Janus nanofibers was composed of oleic acid modified Fe_3O_4 NPs, PVP

90 and DMF (denoted as spinning solutions B). In order to investigate the impact of Fe_3O_4 NPs on the magnetic and fluorescent properties of the Janus nanofibers, various amounts of Fe_3O_4 NPs were introduced into the spinning solutions B, as summarized in Table 1.

95 For comparison, Fe_3O_4/[Dy(BA)_3phen+Eu(BA)_3phen]/PVP composite nanofibers (S_d) were also fabricated by mixing spinning solution A_2 and spinning solution B_1 together at the volume ratio of 1:1 and electrospun via the traditional single-nozzle electrospinning method. This fabrication process of the

100 Fe_3O_4/[Dy(BA)_3phen+Eu(BA)_3phen]/PVP composite nanofibers is an easy way to realize the preparation of the magnetic-fluorescent bifunctional nanofibers.

The compositions and contents of all these spinning solutions, and the products produced by corresponding spinning solutions

105 were listed in Table 1.

Table 1 Compositions of spinning solutions for preparing [Fe_3O_4/PVP]//[(10%Dy(BA)_3phen+n%Eu(BA)_3phen)/PVP]Janus nanofibers (S_{a1-a5}, S_{b1-b5} and S_{c1-c5}) and

110 Fe_3O_4/[Dy(BA)_3phen+Eu(BA)_3phen]/PVP composite nanofibers (S_d), in which n % represents the mass percentage of $Eu(BA)_3$phen to PVP

Journal Name

Dynamic Article Links ▶

ARTICLE TYPE

Samples	Spinning solutions	Compositions					
		Dy(BA)$_3$phen/g	Eu(BA)$_3$phen/g	Fe$_3$O$_4$/g	PVP/g	DMF/g	n %
S$_{a1}$	A$_1$	0.1000	0		1.0000	4.0000	0
	B$_1$			0.2000	1.0000	4.0000	
S$_{a2}$	A$_2$	0.1000	0.0050		1.0000	4.0000	0.5
	B$_1$			0.2000	1.0000	4.0000	
S$_{a3}$	A$_3$	0.1000	0.0100		1.0000	4.0000	1.0
	B$_1$			0.2000	1.0000	4.0000	
S$_{a4}$	A$_4$	0.1000	0.0200		1.0000	4.0000	2.0
	B$_1$			0.2000	1.0000	4.0000	
S$_{a5}$	A$_5$	0.1000	0.0300		1.0000	4.0000	3.0
	B$_1$			0.2000	1.0000	4.0000	
S$_{b1}$	A$_1$	0.1000	0		1.0000	4.0000	0
	B$_2$			0.5000	1.0000	4.0000	
S$_{b2}$	A$_2$	0.1000	0.0050		1.0000	4.0000	0.5
	B$_2$			0.5000	1.0000	4.0000	
S$_{b3}$	A$_3$	0.1000	0.0100		1.0000	4.0000	1.0
	B$_2$			0.5000	1.0000	4.0000	
S$_{b4}$	A$_4$	0.1000	0.0200		1.0000	4.0000	2.0
	B$_2$			0.5000	1.0000	4.0000	
S$_{b5}$	A$_5$	0.1000	0.0300		1.0000	4.0000	3.0
	B$_2$			0.5000	1.0000	4.0000	
S$_{c1}$	A$_1$	0.1000	0		1.0000	4.0000	0
	B$_3$			1.0000	1.0000	4.0000	
S$_{c2}$	A$_2$	0.1000	0.0050		1.0000	4.0000	0.5
	B$_3$			1.0000	1.0000	4.0000	
S$_{c3}$	A$_3$	0.1000	0.0100		1.0000	4.0000	1.0
	B$_3$			1.0000	1.0000	4.0000	
S$_{c4}$	A$_4$	0.1000	0.0200		1.0000	4.0000	2.0
	B$_3$			1.0000	1.0000	4.0000	
S$_{c5}$	A$_5$	0.1000	0.0300		1.0000	4.0000	3.0
	B$_3$			1.0000	1.0000	4.0000	
S$_d$		0.1000	0.0020	0.2000	2.0000	8.0000	

Electrospinning equipments for fabricating Janus nanofibers

[Fe$_3$O$_4$/PVP]//[(10%Dy(BA)$_3$phen+n%Eu(BA)$_3$phen)/PVP] Janus nanofibers were prepared using an electrospinning setup with a homemade parallel spinneret, as indicated in Fig. 1. Two same
5 sized stainless steel needles were used, with the outer diameters of 1.260 mm and inner diameters of 0.900 mm. The two kinds of spinning solutions were respectively loaded into each syringe, and the spinneret was settled vertically. A flat iron net was put about 14 - 16 cm away from the tip of the plastic nozzle to collect
10 the Janus nanofibers. A positive direct current (DC) voltage of 13 - 14 kV was applied between the spinneret and the collector. The electrospinning process was carried out at ambient temperature of 22 - 24 °C and relative air humidity of 44% - 48%. Both the flow rates of the two spinning solutions were measured to be 0.133
15 mL/min. Meanwhile, Fe$_3$O$_4$/[Dy(BA)$_3$phen+Eu(BA)$_3$phen]/PVP composite nanofibers (S$_d$), as a contrast sample, were also prepared to study the superiority of the structure of Janus nanofibers by using the traditional single-spinneret electrospinning setup, and the other spinning parameters were the
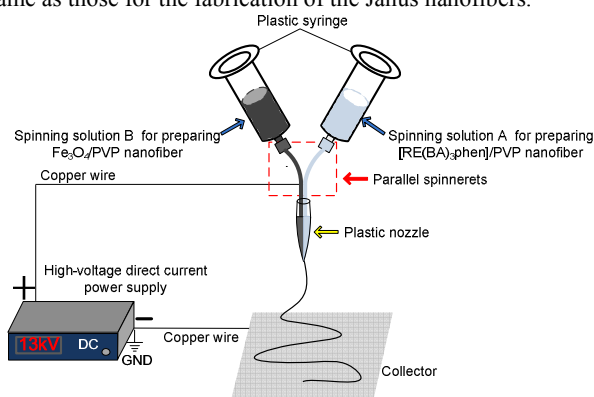20 same as those for the fabrication of the Janus nanofibers.

Fig. 1 Schematic diagrams of the equipments for electrospinning Janus nanofibers
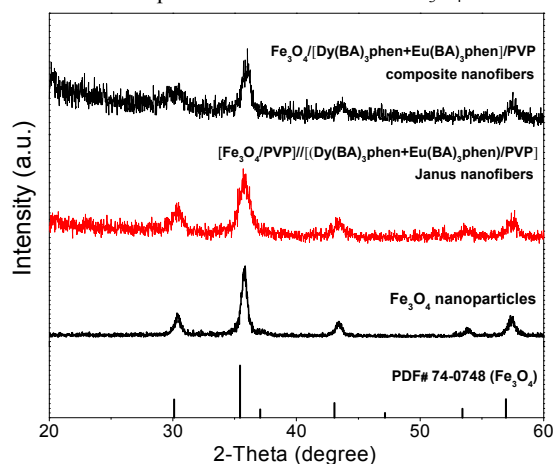
Characterization

25 The as-prepared Fe$_3$O$_4$ NPs, [Fe$_3$O$_4$/PVP]//[(Dy(BA)$_3$phen+

Eu(BA)$_3$phen)/PVP] Janus nanofibers and Fe$_3$O$_4$/[Dy(BA)$_3$phen+ Eu(BA)$_3$phen]/PVP composite nanofibers were identified by an X-ray powder diffractometer (XRD, Bruker, D8 FOCUS) with Cu Kα radiation. The operation voltage and current were kept at 40 kV and 20 mA, respectively. The morphology and internal structure of samples were observed by a field emission scanning electron microscope (FESEM, XL-30) and a transmission electron microscope (TEM, JEM-2010), respectively. The elements analysis for the Janus nanofibers was performed by an energy dispersive spectrometer (EDS, Oxford ISIS 300) attached to the FESEM. The fluorescent properties of the samples were investigated by a Hitachi photoluminescence (PL) spectrophotometer F-7000. The ultraviolet-visible spectrum was determined by suing a UV-1240 ultraviolet-visible spectrophotometer. Then, the magnetic measurements were performed by using a vibrating sample magnetometer (VSM, MPMS SQUID XL). All the measures were performed at room temperature.

Results and discussion

XRD analysis

The phase compositions of the Fe$_3$O$_4$ NPs, [Fe$_3$O$_4$/PVP]//[(Dy(BA)$_3$phen+Eu(BA)$_3$phen)/PVP] Janus nanofibers (S$_{b2}$) and Fe$_3$O$_4$/[Dy(BA)$_3$phen+Eu(BA)$_3$phen]/PVP composite nanofibers (S$_d$) were characterized by means of XRD analysis, as shown in Fig. 2. The XRD patterns of the as-prepared Fe$_3$O$_4$ NPs are conformed to the cubic structure of Fe$_3$O$_4$ (PDF 74-0748), and no characteristic peaks are observed for other impurities such as Fe$_2$O$_3$ and FeO(OH). The diffraction peaks of Fe$_3$O$_4$ in the Janus nanofibers and composite nanofibers are weaker than those of Fe$_3$O$_4$ NPs due to the existence of amorphous PVP and RE complexes in the Janus nanofibers and composite nanofibers. These results demonstrate that the Janus nanofibers and composite nanofibers contain Fe$_3$O$_4$ NPs.
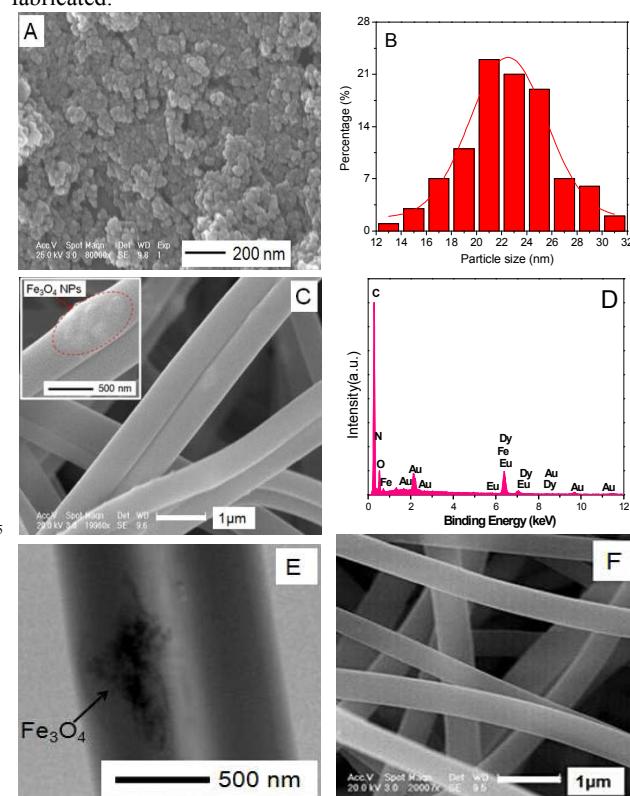

Fig.2 XRD patterns of Fe$_3$O$_4$ NPs, [Fe$_3$O$_4$/PVP]//[(Dy(BA)$_3$phen+Eu(BA)$_3$phen)/PVP] Janus nanofibers and Fe$_3$O$_4$/[Dy(BA)$_3$phen+Eu(BA)$_3$phen]/PVP composite nanofibers

Morphology and structure

The morphology of the as-prepared Fe$_3$O$_4$ NPs was observed by means of SEM, as presented in Fig. 3A. The Fe$_3$O$_4$ NPs are spherical in shape, and the mean diameter of them is 22.50 ± 0.25 nm (Fig. 3B). As shown in Fig. 3C, each [Fe$_3$O$_4$/PVP]//[(Dy(BA)$_3$phen+Eu(BA)$_3$phen)/PVP] Janus nanofiber consists of two nanofibers assembled side-by-side, and the mean diameter of individual nanofiber in the Janus nanofibers is *ca.* 500 nm. Moreover, some Fe$_3$O$_4$ NPs aggregates are faintly visible in one individual nanofiber, whereas the other individual nanofiber is extremely smooth. EDS spectrum shown in Fig. 3D reveals that the Janus nanofibers are composed of elements C, N, O, Dy, Eu, Fe and Au, in which Dy, Eu and Fe elements respectively come from Dy(BA)$_3$phen, Eu(BA)$_3$phen and Fe$_3$O$_4$ NPs, and the Au peak comes from gold conductive film plated on the surface of the sample for SEM observation. Fig. 3E shows the TEM image of a Janus nanofiber. One can see that Fe$_3$O$_4$ NPs are only dispersed in one strand nanofiber. The SEM image of the Fe$_3$O$_4$/[Dy(BA)$_3$phen+Eu(BA)$_3$phen]/PVP composite nanofibers was shown in Fig. 3F. It can be seen that each single composite nanofiber is independent, and the diameter of the composite nanofibers is *ca.* 500 nm. From the above analyses, we can confirm that the [Fe$_3$O$_4$/PVP]//[(Dy(BA)$_3$phen+ Eu(BA)$_3$phen)/PVP] Janus nanofibers have been successfully fabricated.


Fig. 3 SEM image (A) and histogram of diameter (B) of the Fe$_3$O$_4$ NPs; SEM image (C), EDS analysis (D) and TEM image (E) of [Fe$_3$O$_4$/PVP]//[(Dy(BA)$_3$phen+Eu(BA)$_3$phen)/PVP] Janus nanofibers; and SEM image (F) of Fe$_3$O$_4$/[Dy(BA)$_3$phen+ Eu(BA)$_3$phen]/PVP composite nanofibers

Photoluminescence properties

In order to illustrate the advantage of the nanostructure of the magnetic-fluorescent bifunctional Janus nanofibers, the PL spectra of [Fe$_3$O$_4$/PVP]//[(10%Dy(BA)$_3$phen+ 0.5%Eu(BA)$_3$phen)/PVP] Janus nanofibers (S$_{a2}$) and

Fe$_3$O$_4$/[10%Dy(BA)$_3$phen+0.5%Eu(BA)$_3$phen]/PVP composite nanofibers (S$_d$) were contrasted, as shown in Fig. 4. One can see that excitation and emission intensity of the Janus nanofibers are much stronger than those of

5 Fe$_3$O$_4$/[Dy(BA)$_3$phen+Eu(BA)$_3$phen]/PVP composite nanofibers. This result from can be attributed to the isolation of RE complexes from Fe$_3$O$_4$ NPs. From the UV-Vis absorbance spectrum of Fe$_3$O$_4$ NPs illustrated in Fig. 12B, it is observed that Fe$_3$O$_4$ NPs absorb light at ultraviolet wavelengths (<400 nm)

10 much more strongly than visible range (400-700 nm). As illustrated in Fig. 5, Dy(BA)$_3$phen, Eu(BA)$_3$phen and Fe$_3$O$_4$ NPs are promiscuously dispersed in the Fe$_3$O$_4$/[Dy(BA)$_3$phen+Eu(BA)$_3$phen]/PVP composite nanofibers. The exciting light in the composite nanofibers has to pass through

15 Fe$_3$O$_4$ NPs to reach and excite Dy(BA)$_3$phen and Eu(BA)$_3$phen complexes. In this process, a large part of the exciting light has been absorbed by Fe$_3$O$_4$ NPs, and thus the exciting light is much weakened when it reaches the Dy(BA)$_3$phen and Eu(BA)$_3$phen complexes. Similarly, the emitting light emitted by Dy(BA)$_3$phen

20 and Eu(BA)$_3$phen complexes also has to pass through Fe$_3$O$_4$ NPs and is absorbed by them. Consequently, both the exciting and emitting light are severely weakened. For the [Fe$_3$O$_4$/PVP]//[(Dy(BA)$_3$phen+Eu(BA)$_3$phen)/PVP] Janus nanofibers, Dy(BA)$_3$phen, Eu(BA)$_3$phen and Fe$_3$O$_4$ NPs are

25 separated in their own strand, so that the exciting light and emitting light in the [Dy(BA)$_3$phen+Eu(BA)$_3$phen]/PVP strand will be little affected by Fe$_3$O$_4$ NPs. The overall effect is that the [Fe$_3$O$_4$/PVP]//[(Dy(BA)$_3$phen+Eu(BA)$_3$phen)/PVP] Janus nanofibers possess much higher fluorescent performance than the

30 Fe$_3$O$_4$/[Dy(BA)$_3$phen+Eu(BA)$_3$phen]/PVP composite nanofibers.
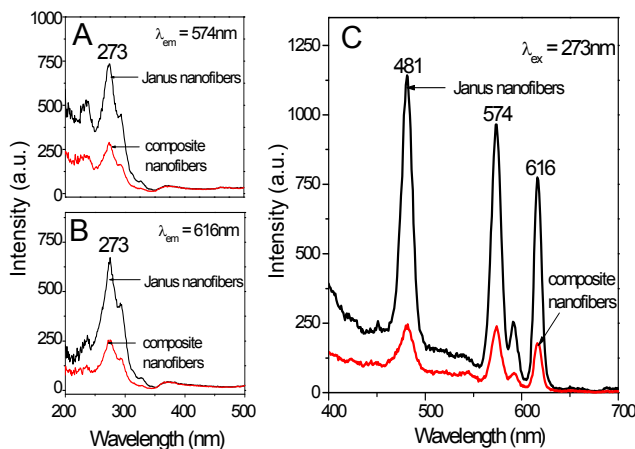
Fig. 4 Excitation spectra monitored at 574nm (A), 616nm (B) and emission spectra (C) of [Fe$_3$O$_4$/PVP]//[(10%Dy(BA)$_3$phen+ 0.5%Eu(BA)$_3$phen)/PVP] Janus nanofibers and

35 Fe$_3$O$_4$/[10%Dy(BA)$_3$phen+0.5%Eu(BA)$_3$phen]/PVP composite nanofibers when the mass ratios of Fe$_3$O$_4$ NPs to PVP were respectively settled at 0.2:1
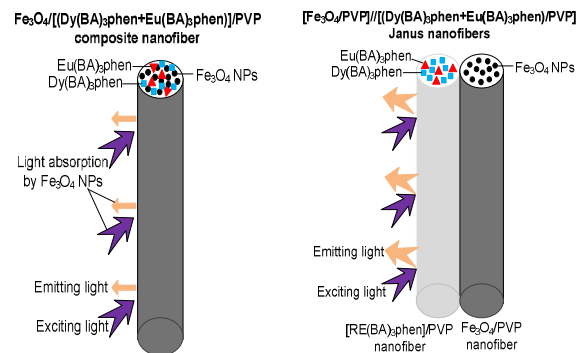
Fig. 5 Schematic diagrams of the exciting light and emitting light

40 in Fe$_3$O$_4$/[Dy(BA)$_3$phen+Eu(BA)$_3$phen]/PVP composite nanofiber and [Fe$_3$O$_4$/PVP]//[(Dy(BA)$_3$phen+Eu(BA)$_3$phen)/PVP] Janus nanofiber

To get the color-tunable Janus nanofibers, the mass percentage

45 of Dy(BA)$_3$phen to PVP were settled as 10 %, and the mass percentage of Eu(BA)$_3$phen to PVP were respectively varied from 0 %, 0.5 %, 1.0 %, 2.0 % to 3.0 % in [(Dy(BA)$_3$phen+ Eu(BA)$_3$phen)/PVP] strand nanofiber. Fig. 6A demonstrates the excitation spectra of the samples monitored at 574 nm (the

50 characteristic emission peak of Dy^{3+}), and the mass ratio of Fe$_3$O$_4$ NPs to PVP was fixed as 0.2:1 (S$_{a1-a5}$). Broad excitation bands extending from 200 to 350 nm are observed in various samples, and the strongest peaks at 273 nm are assigned to the $\pi \rightarrow \pi^*$ electron transition of the ligands.[12] The excitation intensity is

55 decreased with adding more Eu(BA)$_3$phen complexes. Fig. 6B shows the excitation spectra of various samples monitored at 616 nm (the characteristic emission peak of Eu^{3+}). Similarly, the strongest excitation peaks are also located at 273 nm. The excitation intensity is increased along with adding more

60 Eu(BA)$_3$phen complexes. Thus, one can see that both Dy(BA)$_3$phen and Eu(BA)$_3$phen complexes can be simultaneously and most effectively excited using 273-nm single-wavelength ultraviolet light.
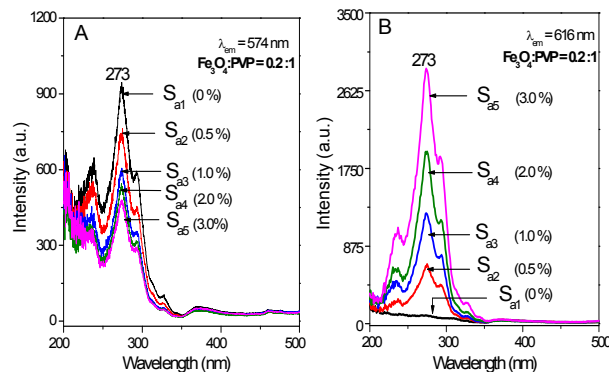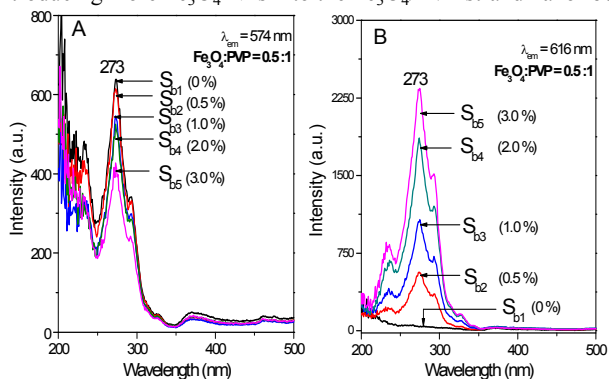

65 **Fig. 6** Excitation spectra of [Fe$_3$O$_4$/PVP]//[(10%Dy(BA)$_3$phen+n%Eu(BA)$_3$phen)/PVP]Janus nanofibers monitored at 574 nm (A) and 616 nm (B) when the mass ratio of Fe$_3$O$_4$ NPs to PVP was fixed at 0.2:1 (S$_{a1}$: n=0, S$_{a2}$: n=0.5, S$_{a3}$: n=1.0, S$_{a4}$: n=2.0, S$_{a5}$: n=3.0)

70 Fig. 7 and Fig. 8 indicate the excitation spectra of the [Fe$_3$O$_4$/PVP]//[(Dy(BA)$_3$phen+Eu(BA)$_3$phen)/PVP] Janus nanofibers containing different amounts of Fe$_3$O$_4$ NPs (S$_{b1-b5}$: Fe$_3$O$_4$:PVP=0.5:1; S$_{c1-c5}$: Fe$_3$O$_4$:PVP=1:1). One can see that both

the Dy(BA)$_3$phen and Eu(BA)$_3$phen complexes can be also simultaneously and most effectively excited using 273-nm single-wavelength ultraviolet light. The excitation intensity of Dy^{3+} (574nm) is decreased with adding more Eu(BA)$_3$phen complexes.
5 On the contrary, the excitation intensity of Eu^{3+} (616nm) is increased along with introducing more Eu(BA)$_3$phen complexes. In addition, by comparing the intensities of the excitation spectra among Fig. 6A, Fig. 7A and Fig. 8A, as well as Fig. 6B, Fig. 7B and Fig. 8B, one can see that the intensity is decreased with
10 introducing more Fe$_3$O$_4$ NPs into the Fe$_3$O$_4$/PVP strand nanofiber.

Fig. 7 Excitation spectra of [Fe$_3$O$_4$/PVP]//[(10%Dy(BA)$_3$phen+n%Eu(BA)$_3$phen)/PVP] Janus nanofibers monitored at 574 nm (A) and 616 nm (B) when the
15 mass ratio of Fe$_3$O$_4$ NPs to PVP was fixed at 0.5:1 (S$_{b1}$: n=0, S$_{b2}$: n=0.5, S$_{b3}$: n=1.0, S$_{b4}$: n=2.0, S$_{b5}$: n=3.0)
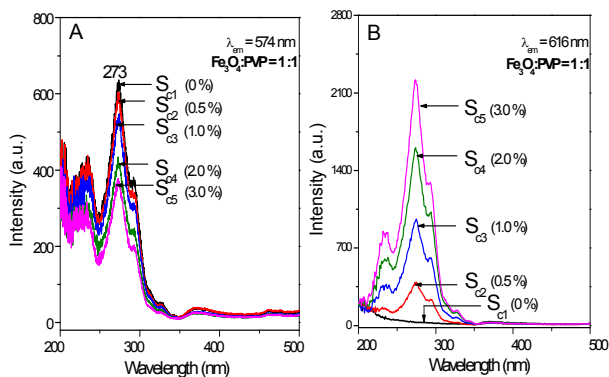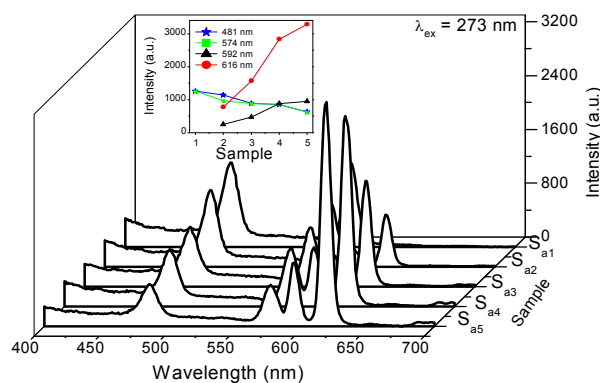

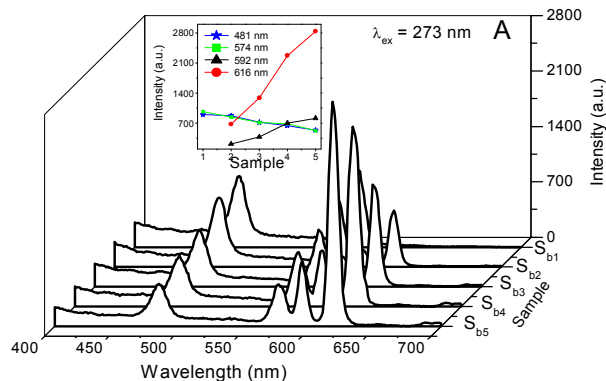**Fig. 8** Excitation spectra of [Fe$_3$O$_4$/PVP]//[(10%Dy(BA)$_3$phen+n%Eu(BA)$_3$phen)/PVP]Janus
20 nanofibers monitored at 574 nm (A) and 616 nm (B) when the mass ratio of Fe$_3$O$_4$ NPs to PVP was fixed at 1:1 (S$_{c1}$: n=0, S$_{c2}$: n=0.5, S$_{c3}$: n=1.0, S$_{c4}$: n=2.0, S$_{c5}$: n=3.0)

The emission spectra of [Fe$_3$O$_4$/PVP]//[(10%Dy(BA)$_3$phen+ n%Eu(BA)$_3$phen)/PVP] Janus nanofibers (from samples S$_{a1}$ to S$_{a5}$)
25 were plotted in Fig. 9. Characteristic emission peaks of the Dy(BA)$_3$phen and Eu(BA)$_3$phen are observed under the most effective excitation of 273-nm ultraviolet light. The blue emission and yellow-green one centering at 481 nm and 574 nm originate respecting from the energy level transition $^4F_{9/2} \rightarrow {}^6H_{15/2}$ and $^4F_{9/2}$
30 $\rightarrow {}^6H_{13/2}$ of Dy^{3+} ions.[38] Meanwhile, two red emitting peaks locating at 592 nm and 616 nm can also be observed, which are respectively ascribed to the energy levels transitions of the $^5D_0 \rightarrow$ $^7F_1$ and $^5D_0 \rightarrow {}^7F_2$ of Eu^{3+} ions, and it is observed that the emission peak at 592 nm is much lower than that at 616 nm.[12]

35 It is interesting and reasonable to suggest that the PL intensity of the Eu^{3+} ions is observed to increase, whereas that of the Dy^{3+} ions is simultaneously found to decrease monotonically with the increase of Eu(BA)$_3$phen concentration. In order to clearly depict the variation trend, the intensities of the characteristic emission
40 peaks of each sample versus different samples were plotted in the inset of Fig. 9. The variation of the PL intensity of the Eu^{3+} and Dy^{3+} can be attributed to the energy distribution. Since the energy that the matrix absorbs and the content of Dy(BA)$_3$phen are constant, more energy is assigned to Eu^{3+} with the increase of
45 Eu(BA)$_3$phen content, thus leading to stronger fluorescence peaks at 592 and 616 nm. Meanwhile, on the contrary, the energy which is assigned to Dy^{3+} is reduced and the fluorescence peaks at 481 and 574 nm are relevantly weakened. Fig. 10 and Fig. 11 respectively show the fluorescent emission spectra of the Janus
50 nanofibers from the samples S$_{b1}$ to S$_{b5}$ and S$_{c1}$ to S$_{c5}$. Similar variable regularity can be observed among Fig. 9, Fig. 10 and Fig. 11, but the overall intensity is decreased with adding more Fe$_3$O$_4$ NPs.


Fig. 9 Comparison among the emission spectra of [Fe$_3$O$_4$/PVP]//[(10%Dy(BA)$_3$phen+n%Eu(BA)$_3$phen)/PVP] Janus nanofibers containing different mass percentage of Eu(BA)$_3$phen complexes when the mass ratio of Fe$_3$O$_4$ NPs to PVP was fixed at 0.2:1 (S$_{a1}$: n=0, S$_{a2}$: n=0.5, S$_{a3}$: n=1.0, S$_{a4}$: n=2.0, S$_{a5}$: n=3.0)
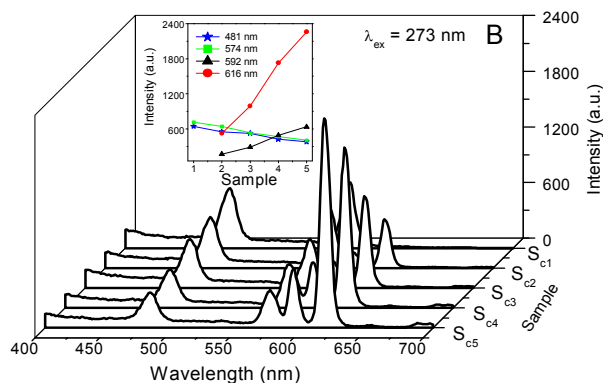
Fig. 10 Comparison among the emission spectra of
[Fe$_3$O$_4$/PVP]//[(10%Dy(BA)$_3$phen+n%Eu(BA)$_3$phen)/PVP] Janus
nanofibers containing different mass percentage of Eu(BA)$_3$phen
complexes when the mass ratio of Fe$_3$O$_4$ NPs to PVP was
respectively fixed at 0.5:1 (A) and 1:1 (B)
(S$_{b1}$: n=0, S$_{b2}$: n=0.5, S$_{b3}$: n=1.0, S$_{b4}$: n=2.0, S$_{b5}$: n=3.0, S$_{c1}$: n=0,
S$_{c2}$: n=0.5, S$_{c3}$: n=1.0, S$_{c4}$: n=2.0, S$_{c5}$: n=3.0)

Generally, color can be represented by the Commission Internationale de L'Eclairage (CIE) 1931 chromaticity coordinates. The CIE chromaticity coordinates for the samples, together with their corresponding photographs upon excitation at 273-nm ultraviolet light, were provided in Table 2 and Fig. 11. As the content of Eu(BA)$_3$phen complexes increases from 0 to 3%, one can see that the fluorescent color of the obtained Janus nanofibers can be easily tuned from greenish blue (S$_{a1}$, S$_{b1}$, S$_{c1}$), white (S$_{a2}$, S$_{b2}$, S$_{c2}$), pale pink (S$_{a3}$, S$_{b3}$, S$_{c3}$), pink (S$_{a4}$, S$_{b4}$, S$_{c4}$) and eventually to yellowish pink (S$_{a5}$, S$_{b5}$, S$_{c5}$). In particular, it is gratify to see that the desirable white emission can be realized by the co-doping of Dy(BA)$_3$phen and Eu(BA)$_3$phen complexes into PVP nanofiber. The results show that the emission color of Janus nanofibers can be turned by adjusting the amount of Eu(BA)$_3$phen complexes.
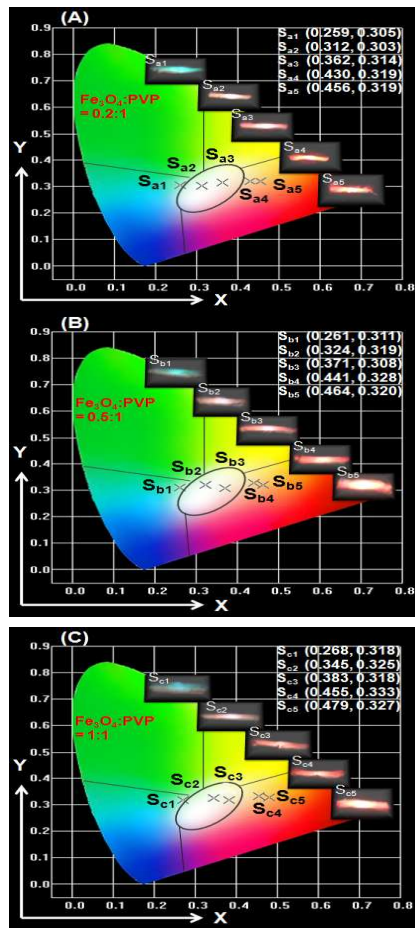
Fig. 11 CIE chromaticity diagram for
[Fe$_3$O$_4$/PVP]//[(10%Dy(BA)$_3$phen+n%Eu(BA)$_3$phen)/PVP] Janus
nanofibers when the mass ratio of Fe$_3$O$_4$ NPs to PVP was
respectively fixed at 0.2:1 (A), 0.5:1 (B), and 1:1 (C), together
with their corresponding photographs upon excitation by 273-nm
ultraviolet light (n = 0, 0.5, 1.0, 2.0, 3.0)

Table 2 Comparison among the CIE chromaticity coordinates (x, y) for the Janus nanofibers excited by 273-nm ultraviolet light

Sample	Sample composition		CIE coordinates	
No.	(n %)	Fe$_3$O$_4$ (g) : PVP (g)	(x, y)	Em (color)
S$_{a1}$		0.2:1	(0.259, 0.305)	
S$_{b1}$	0	0.5:1	(0.261, 0.311)	Greenish blue
S$_{c1}$		1:1	(0.268, 0.318)	
S$_{a2}$		0.2:1	(0.312, 0.303)	
S$_{b2}$	0.5	0.5:1	(0.324, 0.319)	white
S$_{c2}$		1:1	(0.345, 0.325)	
S$_{a3}$		0.2:1	(0.362, 0.314)	
S$_{b3}$	1.0	0.5:1	(0.371, 0.308)	pale pink
S$_{c3}$		1:1	(0.383, 0.318)	
S$_{a4}$		0.2:1	(0.430, 0.319)	
S$_{b4}$	2.0	0.5:1	(0.441, 0.328)	pink
S$_{c4}$		1:1	(0.455, 0.333)	
S$_{a5}$		0.2:1	(0.456, 0.319)	
S$_{b5}$	3.0	0.5:1	(0.464, 0.320)	yellowish pink
S$_{c5}$		1:1	(0.479, 0.327)	

Fig. 12A gives the fluorescent emission spectra (excited by 273 nm) of [Fe$_3$O$_4$/PVP]//[10%Dy(BA)$_3$phen/PVP] Janus nanofibers containing different amounts of Fe$_3$O$_4$ NPs. The [10%Dy(BA)$_3$phen]/PVP strand nanofibers in the Janus nanofibers were fabricated using spinning solution A$_1$, and the Fe$_3$O$_4$/PVP strand nanofiber were fabricated using spinning

solution B_1 (Fe_3O_4: PVP= 0.2: 1), B_2 (Fe_3O_4: PVP= 0.5: 1) and B_3 (Fe_3O_4: PVP = 1: 1), respectively. One can see that the emission intensity of the Janus nanofibers is decreased with adding more Fe_3O_4 NPs into the Fe_3O_4/PVP strand nanofiber due to the light
5 absorption of Fe_3O_4. Moreover, as indicated in Fig. 12C, one can see that the CIE coordinates have slightly variations towards the direction of red color with introducing more Fe_3O_4 NPs. This phenomenon results from that the low-wavelength light is more absorbed by Fe_3O_4 NPs than long-wavelength light, as depicted in
10 Fig. 12B. In other word, red light (616 nm) is less absorbed by Fe_3O_4 NPs compared with cyan light (481 nm). In the inset of Fig. 12A, a standard used for comparison when the mass percentage of Fe_3O_4 to PVP was fixed at 0.2:1 (S_{a1}), compared with the other emission intensity of Janus nanofibers when the mass percentage
15 of Fe_3O_4 to PVP was fixed at 0.5:1 and 1:1, respectively. Reduce the degree of the fluorescent intensity at 481nm is much stronger than the fluorescent intensity at 574nm with the increase of the amount of Fe_3O_4 NPs introduced into Fe_3O_4/PVP nanofiber. In this case, adding more Fe_3O_4 NPs leads to more intense
20 absorption of cyan light, whereas the red light is not absorbed so much. Consequently, the fluorescent color of Janus nanofibers becomes more red with more Fe_3O_4 NPs. Similar phenomena can be observed in the Janus nanofibers containing $Eu(BA)_3phen$ complexes, as seen in Fig. 13 and Fig. 14. The above results
25 indicate that the as-obtained Janus nanofibers can exhibit tunable color and white luminescence in the visible region by changing the content of $Eu(BA)_3phen$ under the excitation of single-wavelength ultraviolet light. In addition, fluorescent color of Janus nanofibers is also influenced by Fe_3O_4 NPs.
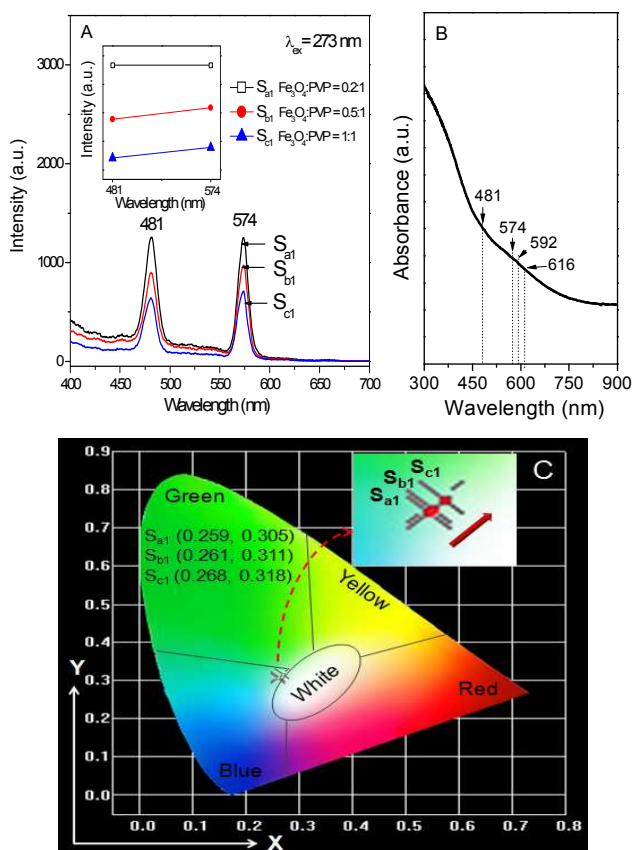

30

Fig. 12 Comparison of emission spectra (A); UV-Vis absorbance

spectrum of Fe_3O_4 NPs (B); and CIE chromaticity diagram (C) for [Fe_3O_4/PVP]//[10%$Dy(BA)_3phen$/PVP] Janus nanofibers
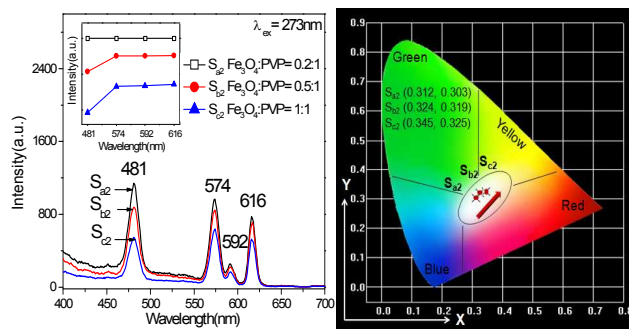35 containing different mass ratios of Fe_3O_4 NPs

Fig. 13 Comparison of emission spectra (left) and CIE chromaticity diagram (right) for [Fe_3O_4/PVP]// [(10%$Dy(BA)_3phen$+0.5%$Eu(BA)_3phen$)/PVP] Janus nanofibers
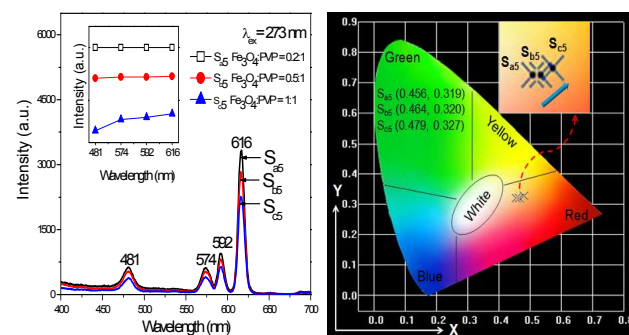40 containing different mass ratios of Fe_3O_4 NPs

Fig. 14 Comparison of emission spectra (left) and CIE chromaticity diagram (right) for [Fe_3O_4/PVP]//
45 [(10%$Dy(BA)_3phen$+3%$Eu(BA)_3phen$)/PVP] Janus nanofibers containing different mass ratios of Fe_3O_4 NPs

The fluorescence decay curves (Fig. 16) of [Fe_3O_4/PVP]//[(10%$Dy(BA)_3phen$+n%$Eu(BA)_3phen$)/PVP] Janus nanofibers containing different mass percentage of $Eu(BA)_3phen$
50 complexes when the mass ratios of Fe_3O_4 to PVP were respectively settled at 0.2:1 (S_{a1-a5}), 0.5:1 (S_{b1-b5}) and 1:1 (S_{c1-c5}) are used to calculate the lifetime and to investigate the fluorescence dynamics of these samples. The samples are excited by 273-nm ultraviolet light and monitored at 574 nm. It is found
55 that the curves follow the single-exponential decay:

$$I_t = I_0\, exp(-t/\iota)$$

where I_t is the intensity at time t, I_0 is the intensity at t = 0 and ι is the decay lifetime. The obtained average lifetime values (τ/ms) of the samples are shown in Fig. 16 (A, B, C). It is obvious that the
60 fluorescence lifetime of the $^4F_{9/2} \rightarrow \,^6H_{13/2}$ transition of Dy^{3+} ions (λ_{em} = 574 nm) in the Janus nanofibers is extended with increase in the content of $Eu(BA)_3phen$ complex. The possible reasons for this result are as follows. The relative content of $Dy(BA)_3phen$ complex in the fibers is reduced with introducing more
65 $Eu(BA)_3phen$. Thus the distance among Dy^{3+} in $Dy(BA)_3phen$ molecular clusters and/or nanoparticles in the Janus nanofibers is increased, resulting in reduction of energy transfer among Dy^{3+} to

Dy^{3+} and elongated fluorescence lifetime of Dy^{3+}.[39]
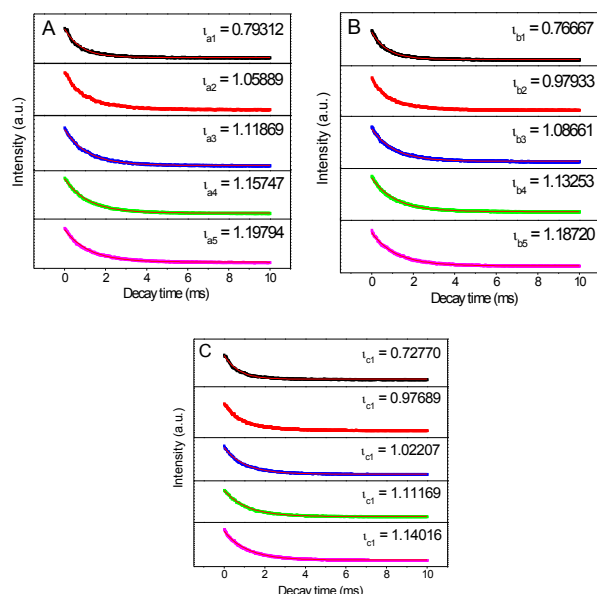
Fig. 16 Fluorescence decay dynamics of the $^4F_{9/2} \rightarrow {}^6H_{13/2}$
transitions (λ_{em} = 574 nm) in Janus nanofibers doped with
different mass percentage of $Eu(BA)_3phen$ complexes when the
mass ratio of Fe_3O_4 NPs to PVP was respectively fixed at
0.2:1(A), 0.5:1(B) and 1:1(C)

Magnetic property

The typical hysteresis loops for
$[Fe_3O_4/PVP]//[(10\%Dy(BA)_3phen+0.5\%Eu(BA)_3phen)/PVP]$
Janus nanofibers containing different mass ratios of Fe_3O_4 NPs
and $Fe_3O_4/[10\%Dy(BA)_3phen+0.5\%Eu(BA)_3phen]/PVP$
composite nanofibers are shown in Fig. 17, and their saturation
magnetizations are listed in Table 3. The saturation magnetization
of the Fe_3O_4 NPs is 48.523 emu·g^{-1}, as indicated in Fig. S2,
Supplementary. It is well known that the saturation magnetization
of a magnetic composite material depends on the mass percentage
of the magnetic substance in the magnetic composite material.[12] It
is found that the saturation magnetization of the magnetic-
fluorescent Janus nanofibers is increased with the increase of the
amount of Fe_3O_4 NPs introduced into the Fe_3O_4/PVP strand.
From the Fig. 17, one can see that hysteresis loops for the Janus
nanofibers (S_{a2}) and composite nanofibers (S_d) were nearly
overlapped, the saturation magnetization of the
$Fe_3O_4/[10\%Dy(BA)_3phen+0.5\%Eu(BA)_3phen]/PVP$ composite
nanofibers (S_d) is 2.629 emu·g^{-1}, which is close to that of the
Janus nanofibers sample S_{a2} (2.660 emu·g^{-1}) because they were
both prepared by spinning solution A_2 and spinning solution B_1.
Combined the analyses of magnetism and fluorescence, it is
found that the Janus nanofibers have the close magnetic property
to the $Fe_3O_4/[Dy(BA)_3phen+Eu(BA)_3phen]/PVP$ composite
nanofibers, but the fluorescent intensity of the Janus nanofibers is
much higher than that of the composite nanofibers, demonstrating
that the novel Janus nanofibers are superior than the composite
nanofibers.
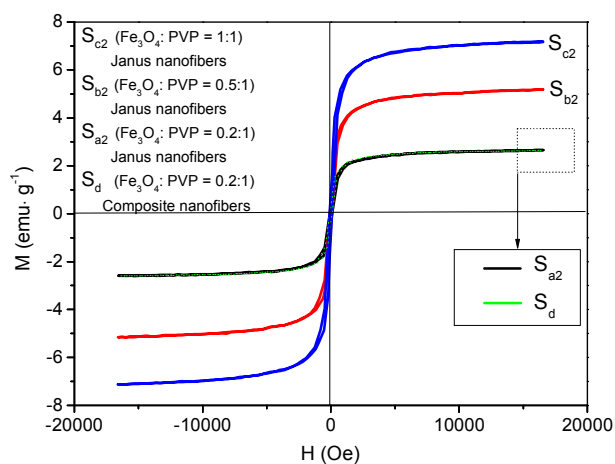
Fig. 17 Hysteresis loops of
$[Fe_3O_4/PVP]//[(10\%Dy(BA)_3phen+0.5\%Eu(BA)_3phen)/PVP]$
Janus nanofibers containing different mass ratios of Fe_3O_4 NPs
and $Fe_3O_4/[10\%Dy(BA)_3phen+0.5\%Eu(BA)_3phen]/PVP$
composite nanofibers

Table 3 Saturation magnetization (Ms) of
$[Fe_3O_4/PVP]//[(10\%Dy(BA)_3phen+0.5\%Eu(BA)_3phen)/PVP]$
Janus nanofibers, and $Fe_3O_4/[10\%Dy(BA)_3phen+$
$0.5\%Eu(BA)_3phen]/PVP$ composite nanofibers

Samples	Ms/emu·g^{-1}
Janus nanofibers (Fe_3O_4:PVP = 0.2:1, S_{a2})	2.660
Janus nanofibers (Fe_3O_4:PVP = 0.5:1, S_{b2})	5.189
Janus nanofibers (Fe_3O_4:PVP = 1:1, S_{c2})	7.164
Composite nanofibers (S_d)	2.629

Conclusions

In summary, novel magnetic and color-tunable bifunctional
$[Fe_3O_4/PVP]//[(Dy(BA)_3phen+Eu(BA)_3phen)/PVP]$ Janus
nanofibers with asymmetry dual-sided structure were successfully
synthesized via electrospinning technique using specifically
designed spinneret. It is very gratifying to see that the new-typed
magnetic-fluorescent bifunctional Janus nanofibers
simultaneously possess both high fluorescent intensity and
saturation magnetization compared with the simply-mixed
$Fe_3O_4/[Dy(BA)_3phen+Eu(BA)_3phen]/PVP$ composite nanofibers.
For the Janus nanofibers, tunable colors from greenish blue to
yellowish pink can be realized by changing the mass ratio of
different RE complexes upon excitation of 273-nm ultraviolet
light, and furthermore, it is the first time to obtain white-light-
emitting magnetic-luminescent bifunctional 1D nanomaterials. In
addition, the color coordinates of the Janus nanofibers have an
obvious variation trend of moving to the direction of red color
with introducing more Fe_3O_4 nanoparticles. Our work has
demonstrated a successful approach to prepare innovation 1D
magnetic and color-tunable nanocomposites with controlled
luminescent and magnetic properties for potential applications in

the realm of future, such as magnetic-luminescent devices, full-color displays, magneto-optic imaging and anti-counterfeit materials, etc.

Acknowledgments

Notes and references

Key Laboratory of Applied Chemistry and Nanotechnology at Universities of Jilin Province, Changchun University of Science and Technology, Changchun 130022. Fax: 86043185383815; Tel: 86043185582574; E-mail: dongxiangting888@163.com
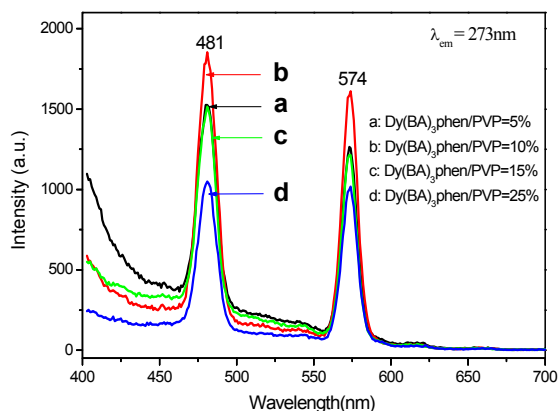
Fig. S1 Emission spectra of Dy(BA)$_3$phen/PVP composite nanofibers containing different mass percentage of Dy(BA)$_3$phen complex
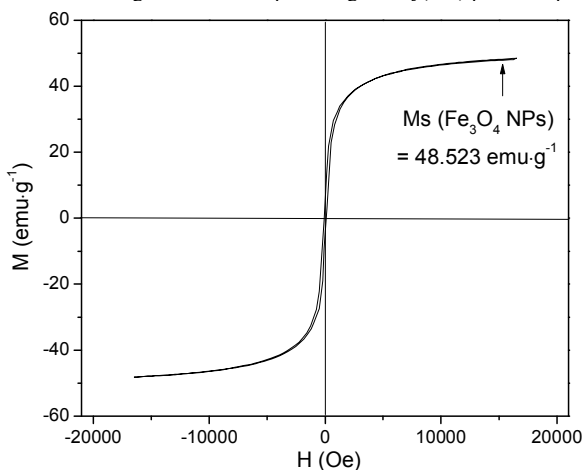

Fig. S2 Hysteresis loops of Fe$_3$O$_4$ NPs

1 J. Y. Han, W. B. Im, D. Kim, S. H. Cheong, G. Lee and D. Y. Jeon, *J. Mater. Chem.,* 2012, **22**, 5374-5381.
2 W. Ahmad, L. J. Zhang and Y. S. Zhou, *CrystEngComm,* 2014, **16**, 3521-3531.
3 K. Diest, J. A. Dionne, M. Spain and H. A. Atwater, *Nano Lett.,* 2009, **9**, 2579-2583.
4 G. S. Lim, H. Kim and J. Y. Chang, *J. Mater. Chem. C,* 2014, **2**, 10184-10188.
5 S. Y. Kim, K. Woo, K. Lim, K. Lee and H. S. Jang, *Nanoscale,* 2013, **5**, 9255-9263.
6 H. X. Guan, G. X. Liu, J. X. Wang, X. T. Dong and W. S. Yu, *New J. Chem.,* 2014, **38**, 4901-4907.
7 H. C. Sun, L. K. Pan, X. Q. Piao and Z. Sun, *J. Mater. Chem. A,* 2013, **1**, 6388-6392.
8 M. Yang, X. D. Zhao, Y. Ji, F. Y. Liu, W. Liu, J. Y. Sun and X. Y. Liu, *New J. Chem.,* 2014, **38**, 4249-4257.
9 S. Som, P. Mitra, V. Kumar, V. Kumar, J. J. Terblans, H. C. Swart and S. K. Sharma, *Dalton Trans.,* 2014, **43**, 9860-9871.
10 L. P. Singh, N. P. Singh and S. K. Srivastava, *Dalton Trans.,* 2015, **44**, 6457-6465.
11 M. N. Luwang, S. Chandra, D. Bahadur and S. K. Srivastava, *J. Mater. Chem.,* 2012, **22**, 3395-3403.
12 Q. L. Ma, J. X. Wang, X. T. Dong, W. S. Yu, G. X. Liu and J. Xu, *J. Mater. Chem.,* 2012, **22**, 14438-14442.
13 A. Son, I. M. Kennedy, K. M. Scow and K. R. Hristova, *J. Environ. Monit.,* 2010, **12**, 1362-1367.
14 Q. L. Ma, J. X. Wang, X. T. Dong, W. S. Yu and G. X. Liu, *Chem. Eng. J.,* 2015, **260**, 222-230.
15 A. Son, D. Dosev, M. Nichkova, Z. Ma, I. M. Kennedy, K. M. Scow and K. R. Hristova, *Anal. Biochem.,* 2007, **370**, 186-194.
16 A. I. Prasad, A. K. Parchur, R. R. Juluri, N. Jadhav, B. N. Pandey, R. S. Ningthoujam and R. K. Vatsa, *Dalton Trans.,* 2013, **42**, 4885-4896.
17 W. Wang, M. Zou and K. Z. Chen, *Chem. Commun.,* 2010, **46**, 5100-5102.
18 H. Y. Chen, D. C. Colvin, B. Qi, T. Moore, J. He, O. T. Mefford, F. Alexis, J. C. Gore and J. N. Anker, *J. Mater. Chem.,* 2012, **22**, 12802-12809.
19 K. Yan, H. Li, X. Wang, C. F. Yi, Q. Y. Zhang, Z. S. Xu, H. B. Xu and A. K. Whittaker, *J. Mater. Chem. B,* 2014, **2**, 546-555.
20 H. G. Wang, Y. X. Li, L. Sun, Y. C. Li, W. Wang, S. Wang, S. F. Xu and Q. B. Yang, *J. Colloid Interface Sci.,* 2010, **350**, 396-401.
21 Q. L. Ma, W. S. Yu, X. T. Dong, J. X. Wang, G. X. Liu and J. Xu, *Opt. Mater.,* 2013, **35**, 526-530.
22 M. M. Moghani and B. Khomami, *Soft Matter,* 2013, **9**, 4815-4821.
23 N. Lv, Q. L. Ma, X. T. Dong, J. X. Wang, W. S. Yu and G. X. Liu, *ChemPlusChem,* 2014, **79**, 690-697.
24 X. Xi, Q. L. Ma, M. Yang, X. T. Dong, J. X. Wang, W. S. Yu and G. X. Liu, *J. Mater. Sci.: Mater. Electron.,* 2014, **25**, 4024-4032.
25 F. Bi, X. T. Dong, J. X. Wang and G. X. Liu, *RSC Adv.,* 2015, **5**, 12571-12577.
26 R. Sahay, P. S. Kumar, R. Sridhar, J. Sundaramurthy, J. Venugopal, S. G. Mhaisalkar and S. Ramakrishna, *J. Mater. Chem.,* 2012, **22**, 12953-12971.
27 K. A. Rieger, N. P. Birch and J. D. Schiffman, *J. Mater. Chem. B,* 2013, **1**, 4531-4541.
28 S. J. Choi, C. Y. Choi, S. J. Kim, H. J. Cho, S. Jeon and II-Doo Kim, *RSC Adv.,* 2015, **5**, 7584-7588.
29 I. N. Strain, Q. Wu, A. M. Pourrahimi, M. S. Hedenqvist, R. T. Olsson and R. L. Andersson, *J. Mater. Chem. A,* 2015, **3**, 1632-1640.
30 X. Y. Wang, C. Drew, S. H. Lee, K. J. Senecal, J. Kumar and L. A. Samuelson, *Nano Lett.,* 2002, **2**, 1273-1275.
31 S. C. Baker, N. Atkin, P. A. Gunning, N. Granville, K. Wilson, D. Wilson and J. Southgate, *Biomaterials,* 2006, **27**, 3136-3146.
32 S. L. Chen, H. Q. Hou, F. Harnisch, S. A. Patil, A. A. C. Martinez, S. Agarwal, Y. Y. Zhang, S. S. Ray, A. L. Yarin, A. Greiner and U. Schroder, *Energy Environ. Sci.,* 2011, **4**, 1417-1421.
33 R. Sridhar, R. Lakshminarayanan, K. Madhaiyan, V. A. Barathi, K. H. C. Lim and S. Ramakrishna, *Chem. Soc. Rev.,* 2015, **44**, 790-814.

34 P. S. Kumar, J. Sundaramurthy, S. Sundarrajan, V. J. Babu, G. Singh, S. I. Allakhverdiev and S. Ramakrishna, *Energy Environ. Sci.,* 2014, **7**, 3192-3222.

35 H. A. Khorami, A. Eghbali, M. Keyanpour-Rad, M. R. Vaezi and M. Kazemzad, *J. Mater. Sci.,* 2014, **49**, 685-690.

36 Y. Y. Zheng, X. B. Wang, L. Shang, C. R. Li, C. Cui, W. J. Dong, W. H. Tang and B. Y. Chen, *Mater. Charact.,* 2010, **61**, 489-492.

37 S. B. Meshkova, *J. Fluoresc.,* 2000, **10**, 333-337.

38 S. Dutta, S. Som and S. K. Sharma, *RSC Adv.,* 2015, **5**, 7380-7387.

39 R. Bonzanini, D. T. Dias, E. M. Girotto, E. C. Muniz, M. L. Baesso, J. M. A. Caiut, Y. Messaddeq, S. J. L. Ribeiro, A. C. Bento and A. F. Rubira, *J. Lumin.,* 2006, **117**, 61-67.